Coaxial-resonator-driven rf (Paul) trap for strong confinement

S. R. Jefferts, C. Monroe, E. W. Bell,* and D. J. Wineland
National Institute of Standards and Technology, Boulder, Colorado 80303
(Received 22 August 1994)

We describe a variant of the quadrupole rf (Paul) ion trap capable of localization of a trapped ion to much less than an optical wavelength (Lamb-Dicke regime). The trapping potentials are generated by a high-Q, vacuum-compatible, quarter-wave resonator driven at about 240 MHz. The binding strength of the trap has been characterized. The trap contains compensation electrodes which allow the cancellation of stray static electric fields within the trap. Secular frequencies of tens of megahertz have been achieved for trapped magnesium and beryllium ions.

PACS number(s): 32.80.Pj

I. INTRODUCTION

In this paper we describe an ion trap apparatus capable of very strong confinement. Strong confinement is important in several applications. In optical atomic spectroscopy, strong confinement allows the attainment of the Lamb-Dicke condition whereby the extent of the atom's motion is less than $\lambda/2\pi$, where λ is the wavelength of the exciting radiation [1]. Attainment of the Lamb-Dicke condition is important because it suppresses broadening due to the first-order Doppler effect, which, in harmonically bound atoms, takes the form of motion-induced sidebands [2–5]. It also suppresses the fluctuations of the "carrier" from measurement to measurement [6]. More recently, strong confinement has been suggested as a way to observe the effects of super and subradiance for two closely spaced atoms under well-controlled conditions [7]. Achievement of the Lamb-Dicke limit also suggests experiments on single-atom cavity QED and nonclassical atomic fluorescence features under controlled conditions [8,9].

With strong confinement, we should be able to achieve resolved sideband cooling [10,11] using allowed electric-dipole transitions. Previously, resolved sideband cooling has been achieved using weakly allowed optical transitions [11]. For resolved sideband cooling, we require that the trap is made deep enough that the atom oscillation frequencies (ω_i, $i=x,y,z$) satisfy $\omega_i \gg \gamma$, where γ is the linewidth of the transition. Use of resolved sidebands on allowed electric-dipole transitions has the potential advantage that cooling to the ground state of motion can be achieved very rapidly. Resolved sidebands should also facilitate precise measurement of the lifetimes of rapidly decaying levels by measuring the linewidth of the resolved carrier.

In a Penning trap [12], single-ion confinement is limited by the strength of binding along the magnetic-field direction, which we can characterize by the (harmonic) binding frequency ω_z. For stable trapping in the radial direction, we must have $\omega_z < \omega_c/\sqrt{2}$, where ω_c is the ion cyclotron frequency. This implies $2\pi\nu_z \equiv \omega_z < 2^{-1/2}QB/M$, where Q is the ion charge, B is the magnetic-field strength, and M is the ion mass. For $B=10$ T, $Q=1e$, and $M=9$ u (e.g., $^9Be^+$), $\nu_z < 12$ MHz. In this paper, we discuss only the Paul trap because, for practical field strengths, the binding should be stronger.

For a single ion bound in a quadrupole rf Paul trap [12], the axial or z frequency ω_z must satisfy $\omega_z \leq \Omega/2$, where Ω is the rf drive frequency. If we assume that the static potential applied between the electrodes is zero, then, at the Mathieu stability limit ($q_z=0.908$) [12,13] in an axially symmetric trap, $\omega_z(\max)=\Omega/2$ and the radial secular frequency is given by $\omega_r(\max)\simeq 0.35\omega_z(\max)$. The maximum secular frequencies can then be characterized by the expression for $\nu_z(\max)$ [12,13]

$$\nu_z(\max)=\frac{\Omega/2\pi}{2}=\frac{1}{2\pi d_0}\left[\frac{QV_0}{0.908M}\right]^{1/2}, \quad (1)$$

where Q is the ion charge, V_0 is the peak rf potential applied between the ring and end caps, M is the ion mass, and d_0 is the characteristic trap dimension. For a trap with hyperbolic electrodes, $2d_0^2 \equiv r_0^2 + 2z_0^2$, where r_0 is the inner radius of the ring electrode and $2z_0$ is the inner end-cap to end-cap distance. Using $Q=1e$, $M=9$ u, $V_0=2$ kV, and $d_0=0.15$ mm, we find $\nu_z(\max)\simeq 164$ MHz and $\nu_r(\max)\simeq 58$ MHz. These conditions would allow resolved sidebands on the $S\rightarrow P$ transition in $^9Be^+$, where $\gamma/2\pi=19.4$ MHz. If we assume $\nu_r=58$ MHz and the ion is cooled to the ground sate of motion, the Lamb-Dicke parameter is $2\pi x_0/\lambda=0.063$, where x_0 is the spread of the zero-point wave function.

From Eq. (1), to achieve strong confinement, we require large values of V_0 and small values of d_0. Implicitly, we assume that Ω is adjusted to give stable trapping, that is, $\Omega > 2\omega_z$. Large values of V_0 can be limited by electric-field breakdown or arcing. Also, if the high voltage is generated external to the required vacuum enclosure for the trap, the voltage at the trap is reduced by the capacitance of the vacuum feedthroughs. This problem becomes more difficult for the required high values of Ω.

As the trap dimensions are reduced, it becomes more

*Present address: National Institute of Standards and Technology, Building 221, Gaithersburg, MD 20899.

difficult to machine the desired electrode shapes. This problem can be minimized by using simpler electrode shapes where the leading anharmonic terms in the trap potential can be nulled for appropriate electrode shapes. For example, nominally quadrupolar electrodes with simple conical surfaces can be used [14]. "Planar" traps formed with holes in parallel plates [15,16] or with conducting rings [16] simplify construction even further. These electrodes have the advantage that they can be made small by using lithographic techniques [16].

As multielectrode traps (such as the conventional quadrupole trap) become smaller, the relative electrode positions also become more difficult to maintain. One way to eliminate this problem is to keep either the ring or end-cap electrodes small and let the complementary electrode(s) recede to large distances. The Paul-Straubel or "ring" trap [17] is essentially a ring electrode with the end caps at large distances. This trap has been analyzed [16,18,19] and demonstrated for Ba^+ ions [18] and In^+ ions [19]. For this kind of trap, an efficiency ϵ can be defined as the ratio of the rf voltage required in a quadrupole trap with hyperbolic electrodes to the voltage required in the ring trap (of the same internal ring diameter) which gives the same secular frequency. References [16,18,19] find ϵ in the range of 0.1–0.2. In a similar spirit, Janik, Prestage, and Maleki [20] have analyzed the case of a linear trap with two and three electrodes rather than four electrodes as for the quadrupole linear trap. For the two-electrode trap they find $\epsilon \simeq 0.25$.

The "end-cap" trap is complementary to the Paul-Straubel trap in that it has closely spaced end cap electrodes with the ring receding to infinity. Schrama *et al.* [19] analyzed and demonstrated a version of this trap using Mg^+ ions. They find an efficiency ϵ in the range of 0.2–0.5. Both the Paul-Straubel or ring trap and the end-cap trap additionally provide a more open optical access for collecting ion fluorescence light than the conventional quadrupole trap.

In the work described below [21], we discuss a strategy for achieving large values of V_0 and Ω and small values of d_0 in a trap with nominal quadrupolar geometry where $\epsilon \simeq 1$.

II. DESCRIPTION

The trap described here is very simple; it consists of two thin sheets of metal: the first, the ring, has a hole, the second, perpendicular to the first, has a slit and acts as the end caps. The arrangement is illustrated in Fig. 1. One trap constructed with this geometry is used for trapping $^{24}Mg^+$ ions and has a ring inner diameter $2r_0$ of 0.43 mm. The end-cap slit width $2z_0$ is 0.32 mm. The molybdenum sheet from which the trap was constructed was 0.13 mm thick. As shown in Fig. 1, the relative position of the trap electrodes is maintained by ceramic positioning rods.

The trap is mounted at the end of an ultrahigh-vacuum-compatible coaxial quarter-wave resonant transmission line. This oxygen-free high-conductivity copper quarter-wave line is installed inside a vacuum enclosure which has fused silica windows to allow the passage of uv laser beams for cooling and probing the atom and resonance fluorescence light from the ions. The transmission line is resonant at a frequency of approximately 240 MHz and has an unloaded quality factor Q_u on the order of 2000. The transmission line is excited with a small loop antenna at the base of the transmission line. The area of the loop is adjusted so that, on resonance, the antenna plus resonator presents a 50-Ω load to the driving amplifier. With some care adjusting the coupling, voltage standing-wave ratios of less than 1.05 can be achieved. With 1 W of incident rf power, the calculated rf trapping voltage V_0 at the trap is about 700 V peak, neglecting the trap capacitance and end effects of the resonator. From the modeled trap parameters (Sec. III) and the measured secular frequencies (below), we calculate the actual voltage between the ring and end caps to be $V_0 \simeq 600$ V for 1 W of incident power. We have been unable to apply voltage much beyond 1 kV due to a vacuum discharge problem which we are attempting to solve.

One advantage of this type of design results from the fact that the rf voltage at the vacuum feedthrough is small, thus minimizing problems associated with high-voltage breakdown at or before the feedthrough as well as reduction of the resonator Q by the vacuum feedthrough. An extension of the design would be to mount the "ring" electrode at the antinode of a half-wave transmission line resonator with the end caps attached to the outer wall of the transmission line. This geometry would allow a direct current to be passed through the ring electrode to evaporate any contaminants on the trap ring [18].

Uncontrolled static electric fields arising from contact potentials or charged patches can cause significant problems in miniature rf traps. These fields displace ions from the zero of the rf trapping fields, thereby leading to undesirable increases in the "micromotion" amplitudes [18]. A common scheme for dealing with these problems is the introduction of "compensation electrodes," which are used to cancel the stray electric fields in the trapping regions. We have included compensation electrodes, similar to those used by Nagourney [22], in the manner shown in Fig. 1. Static potentials applied to various combinations of the compensation electrodes allow for cancellation of static electric fields in an arbitrary direction in the trapping region.

With zero static potential between the electrodes and in the pseudopotential approximation, the secular (motional) frequencies of a trapped ion can be expressed as

$$\omega_i = \alpha_i \frac{\sqrt{2} Q V_0}{m d_0^2 \Omega} , \tag{2}$$

where α_i is a numerical constant for ion motion along the ith axis ($i = x,y,z$; see Fig. 1). In the case of a quadrupolar hyperbolic ion trap, the constant α_i is $\frac{1}{2}$ for the x and y directions and 1 for the z direction. The trap described here breaks the symmetry about the z direction, causing $\omega_x < \omega_y$. In the pseudopotential approximation, with zero static electric field between the trap electrodes, $\omega_x + \omega_y = \omega_z$. Measured ion motional frequencies for this trap fall in the ratios of $\omega_x/\omega_z = 0.40$ and $\omega_y/\omega_z = 0.60$.

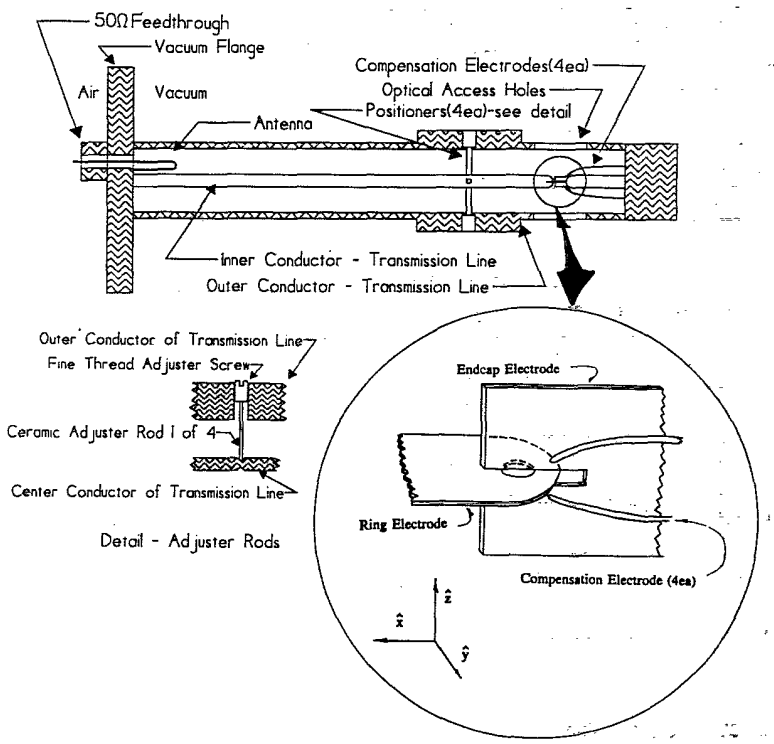

FIG. 1. Approximate scale drawing of the coaxial resonator and rf trap electrodes (shown in an expanded view in the lower right of the figure). The ring electrode is attached to the inner conductor at the position of the antinode of the quarter-wave line. The end cap electrode is held near the rf ground by the short section of center conductor at the right-hand side of the resonator. The resonator is driven by a coaxial line external to the vacuum system shown at the left. The area of the loop antenna is adjusted so the resonator (on resonance) presents a matched load (50 Ω) to the input line. The resonator is surrounded by a vacuum envelope (not shown in the figure) which has quartz windows to allow the passage of uv laser beams and fluorescence light. The position of the ring electrode relative to the end cap electrode is maintained by four adjustable ceramic rods (alumina) shown in the detail in the lower left of the figure. Static potentials are applied to four compensation electrodes to compensate for stray electric fields due to contact potentials and charge buildup on the trap electrodes. For a proper selection of compensation potentials, the average position of a single trapped ion coincides with the position of a zero rf electric field. The two compensation electrodes in front of the end cap electrode are shown in the expanded view in the lower right of the figure. Two more compensation electrodes (behind the end cap electrode) are not shown in the figure.

The secular frequencies of trapped $^{24}Mg^+$ ions were measured by monitoring the intensity of scattered laser-cooling light ($\lambda \simeq 280$ nm) as an rf drive was applied to one of the compensation electrodes and swept over the frequency range which included the secular motion frequencies. Data taken with a single trapped $^{24}Mg^+$ ion and $V_0 \simeq 450$ V at frequency Ω are shown in Fig. 2. The measurements of ion secular frequencies at a given rf voltage in Ω yield the efficiency of this trap relative to the normal hyperbolic rf trap. From these measurements, we can assign a trap efficiency factor ϵ of about 0.9 for the axial (z) direction of this trap. This compares favorably with the efficiency factor of about 0.13 for the single-ring trap [18] and between 0.2 and 0.5 for the multiring trap [16], or end cap trap [19]. We have constructed a similar but slightly smaller trap ($r_0 = 0.15$ mm, $z_0 = 0.10$ mm), for $^9Be^+$ ions; this trap has demonstrated confinement with secular axial frequencies in excess of 50 MHz ($\Omega/2\pi = 230$ MHz), the largest secular frequency reported to date to our knowledge. Previously, secular frequen-

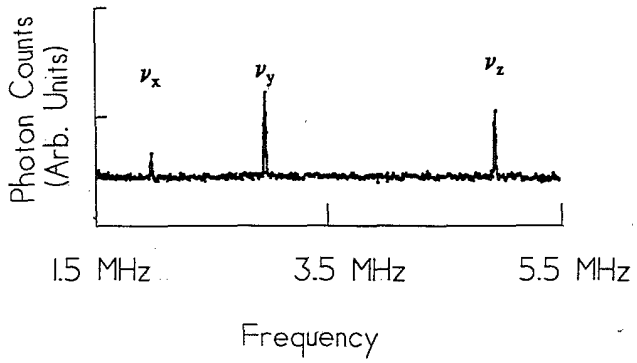

FIG. 2. Response of a single $^{24}Mg^+$ ion to an oscillating potential applied to one of the compensation electrodes shown in Fig. 1. The cooling laser for $^{24}Mg^+$ ions is tuned several linewidths to the red of the $^2S_{1/2} \rightarrow {}^2P_{3/2}$ transition. When the ion is excited by the oscillating electric field, the Doppler shift caused by its increased velocity leads to an increase in fluorescence scattering. The three resonances shown correspond to excitation of the three secular frequencies ω_x, ω_y, and ω_z.

cies of approximately 10 MHz have been reported for Ba^+ ions [16,18]. In this second trap the secular frequency was inferred by measuring the ion-ion spacing at low rf-drive levels, which calibrates the "spring" constant of the trap, and then scaling the spring constant to higher rf-trapping voltages. This measurement, coupled with the modeled electric potential in the trap (below) and the results from the first trap using trapped $^{24}Mg^+$, allows the assignment of the secular frequencies at arbitrary values of the rf-trapping voltage. The secular frequencies will be limited by the requirement that $\omega_z < \Omega/2$ for stable trapping (Mathieu stability limit). To increase ω_z, one must increase Ω; one way this can be accomplished with no change to the apparatus is by driving the transmission line at the first overtone, thereby raising Ω, and hence the limit on ω_z, by a factor of 3.

III. MODELING

This trap design does not lend itself well to analytic methods of solution for the electric potential in the trapping region, so the trap potential must be modeled using a computer program which can describe the full three-dimensional extent of the trap electrodes. We have performed modeling of the three-dimensional trap structure using the MAFIA [23] computer program.

The ring and end-cap electrodes of the $^{24}Mg^+$ trap were discretized on a cubical mesh whose overall side was 1.02 mm on a side with a distance between individual mesh points of 0.013 mm. The mesh axes lay along the same coordinate system as the trap coordinate system shown in Fig. 1, with the origin centered on the trap. The compensation electrodes were not included in the model. The mesh spacing was chosen so there were a sufficient number of mesh points to describe the smallest feature of the trap. The electrostatic field was then calculated and the secular frequencies determined from the field. The calculated motional frequencies are in the ratios $\omega_x/\omega_z = 0.44$ and $\omega_y/\omega_z = 0.63$, in reasonable agreement with the measured ratios of $\omega_x/\omega_z = 0.40$ and $\omega_y/\omega_z = 0.60$. The relatively coarse grid used in the trap modeling limits the accuracy of the modeled trap potential thus causing the calculated ω_x and ω_y to not sum exactly to ω_z.

Higher-order terms in the potential are also of importance. These have also been estimated by fitting the MAFIA results to the expansion (in spherical coordinates)

$$\Phi(r,\theta,\phi) = V_0 \sum_{n=0}^{\infty} C_{2n} \left[\frac{r}{d_0}\right]^{2n} P_{2n}(\cos\theta) \ . \qquad (3)$$

As a result of the reflection symmetry in $\hat{z}$, the odd order terms in the expansion have been eliminated. The constant C_2 is the coefficient of the quadrupolar trapping potential and is of order 1. The C_4 term in the expansion, the lowest-order correction to the described quadrupole potential, is less than 0.3. Higher-order even terms in the expansion have not been calculated.

Due to the small size of the trap, significant misalignment of the trap electrodes is a possibility. To determine the sensitivity of the trapping potential to this effect, possible misalignments of the components of the trap were modeled. Several cases where the end caps were shifted up to 0.13 mm relative to the ring in the y and z directions were computed. This distance corresponds to about one-third of the ring diameter and represents a "worst" case misalignment. The predicted motional frequencies for maximal misalignment differed by less than 5% from the frequencies for the aligned case. This calculated shift is approximately the uncertainty introduced due to discretizing the trap on the finite mesh used. Therefore, it seems that small misalignments of the trap electrodes do not significantly alter the characteristics of the trap.

IV. CONCLUSIONS

This trap has demonstrated the highest secular frequencies for trapped ions reported to date and can be extended to even higher frequencies. Unlike some other designs, it retains the trapping efficiency of conventional hyperbolic quadrupolar designs, thereby allowing larger traps to be built to achieve a given secular frequency and thus relaxing dimensional tolerance requirements. Use of a coaxial-resonator-based design minimizes problems associated with high-voltage breakdown and facilitates the attainment of high values of the drive frequency Ω.

ACKNOWLEDGMENTS

Support for this project has been provided by the ONR. S.R.J. and C.M. received financial support from the National Research Council. We thank J. C. Bergquist for help in setting up the cooling laser used in these experiments. A. S. Barton provided significant help in the early stages of this work. We thank the AT-7 code group at Los Alamos National Laboratories for the use of the MAFIA modeling program. We thank R. Blatt, J. Miller, and M. Young for helpful comments on the manuscript.

[1] R. H. Dicke, Phys. Rev. **89**, 472 (1953).

[2] D. J. Wineland and W. M. Itano, Phys. Rev. A **20**, 1521 (1979); J. C. Bergquist, W. M. Itano, and D. J. Wineland, *ibid.* **36**, 428 (1987).

[3] W. Neuhauser, M. Hohenstatt, P. E. Toschek, and H. G. Dehmelt, Phys. Rev. A **22**, 1137 (1980).

[4] G. Janik, W. Nagourney, and H. Dehmelt, J. Opt. Soc. Am. **2**, 1251 (1985).

[5] A. A. Madej, K. J. Siemsen, J. D. Sankey, R. F. Clark, and J. Vanier, IEEE Trans. Instrum. Meas. **42**, 234 (1993).

[6] H. Dehmelt, Bull. Am. Phys. Soc. **18**, 1521 (1973).
[7] R. G. Devoe and R. G. Brewer, Bull. Am. Phys. Soc. **38**, 1140 (1993).
[8] *Fundamental Systems in Quantum Optics,* Proceedings of the Les Houches Summer School of Theoretical Physics, Session LIII, Les Houches, France, 1990, edited by J. Dalibard, J. M. Raimond, and J. Zinn-Justin (Elsevier, Amsterdam, 1992).
[9] W. Vogel, Phys. Rev. Lett. **67**, 2450 (1991); W. Vogel and R. Blatt, Phys. Rev. A **45**, 3319 (1992).
[10] D. J. Wineland and H. Dehmelt, Bull. Am. Phys. Soc. **20**, 637 (1975).
[11] F. Diedrich, J. C. Bergquist, W. M. Itano, and D. J. Wineland, Phys. Rev. Lett. **62**, 403 (1989).
[12] H. G. Dehmelt, Adv. At. Mol. Phys. **3**, 53 (1967); **5**, 109 (1969); D. J. Wineland, W. M. Itano, and R. S. Van Dyck, Jr., *ibid.* **19**, 135 (1983); R. C. Thompson, *ibid.* **31**, 63 (1993).
[13] R. F. Wuerker, H. Shelton, and R. V. Langmuir, J. Appl. Phys. **30**, 342 (1959).
[14] E. C. Beaty, J. Appl. Phys. **61**, 2118 (1987).
[15] M. H. Prior and H. A. Shugart, Phys. Rev. Lett. **27**, 902 (1971).
[16] R. G. Brewer, R. G. DeVoe, and R. Kallenbach, Phys. Rev. A **46**, R6781 (1992).
[17] H. Straubel, Naturwissenschaften **18**, 506 (1955).
[18] N. Yu, W. Nagourney, and H. Dehmelt, J. Appl. Phys. **69**, 3779 (1991).
[19] C. A. Schrama, E. Peik, W. W. Smith, and H. Walther, Opt. Commun. **101**, 32 (1993).
[20] G. R. Janik, J. D. Prestage, and L. Maleki, J. Appl. Phys. **67**, 6050 (1990).
[21] S. R. Jefferts, C. Monroe, A. S. Barton, and D. J. Wineland, Bull. Am. Phys. Soc. **39**, 1167 (1994).
[22] W. Nagourney (private communication).
[23] T. Weiland, MAFIA (Release 3.1), October 1991, CST, Ohlystrasse 69, D-6100 Darmstadt, Germany.